Protein adsorption at the air-water interface by a charge sensing interferometric technique.

Paola Brocca,*,† Andrea Saponaro,‡ Bianca Introini,‡ Valeria Rondelli, † Martina Pannuzzo°, Domenica Raciti,‖ Mario Corti,§ and Antonio Raudino*,‖

†Department of Biotechnology and Translational Medicine, University of Milan, Italy
‡ Department of Biosciences, University of Milan, Italy
°IIT, Genova, Italy
§CNR-IPCF, Messina, Italy
‖Department of Chemical Sciences, University of Catania, Italy

Corresponding authors:

Paola Brocca
Dept. Medical Biotechnology and Translational Medicine.
University of Milano.
LITA. Via F.lli Cervi, 93, 20090 Segrate (MI), Italy.
tel: +39 02 503 30351 - Fax: +39 02 503 30365
paola.brocca@unimi.it

Antonio Raudino
Department of Chemical Sciences, University of Catania,
Viale Andrea Doria, 6 - 95125 Catania, Italy
tel: +39 095 7385078- Fax: +39 095 580138
araudino@dipchi.unict.it

ABSTRACT:

Protein uptake at the interface of a millimeter-sized air bubble in water, is investigated by a recently developed differential interferometric technique. The technique allows the study of capillary waves with amplitudes in the range of 10^{-9} m, excited at the surface of the bubble by an electric field of intensity in the order of 10 V/cm. By studying the resonant modes of the bubble (radial and shape modes) it is

possible to assess variations of interfacial properties and, in particular, of the net surface charge as a function of bulk protein concentration. Sensing the interfacial charge, the technique enables us to follow the absorption process in condition of low concentrations, not easily assessable by other methods. We focus on bovine serum albumin (BSA) and Lysozyme, as representatives of typical globular proteins. To provide a comprehensive insight into the novelty of the technique we also investigated the equilibrium adsorption of SDS ionic surfactant for bulk concentrations hundreds times lower than the CMC. Results unveil how the absorption of charged molecules affects the amplitudes of the bubble resonant modes even before affecting the frequencies in a transition-like fashion. Different adsorption models are proposed and developed. They are validated against the experimental findings by comparing frequency and amplitude data. By measuring the charging rate of the bubble interface, we have followed the absorption kinetics of BSA and Lysozyme recognizing a slow, energy barrier limited, phenomena, with characteristic times in agreement with data in the literature. The evaluation of the surface excess concentration (Γ) of BSA and SDS at equilibrium is obtained by monitoring charge uptake. At the investigated low bulk concentrations, reliable comparisons with literature data from equilibrium surface tension isotherm models, are reported.

1. INTRODUCTION

The determination of interfacial characteristics of the air/water interface in the presence of proteins in solution is crucial in many applied fields. In particular, the knowledge about the initial steps of adsorption processes is having large relevance for applications in food, pharmaceutics, and cosmetics allowing the optimization of the initial active surfactant concentration, both in traditional and innovative applications.[1-3,4-6] The growing interest in biofilms formation and features investigation has enlarged the importance of characterizing interfaces in the presence of high molecular weight proteins to mimic biological systems.[7-8] Surface stabilization of air/liquid and liquid/liquid systems is controlled by the adsorption processes of active molecules at the interface and their interactions. Information on structural arrangement and interactions among adsorbed molecules are difficult to assess experimentally at a molecular level. Techniques as vibrational sum-frequency generation and neutron and x-ray scattering [ref] are applied to give information at this scale. An important parameter that depends on the molecular layer of water, surfactant, proteins and ions at the interface, is the interfacial charge. Charge is

Formattato: Non Evidenziato

Formattato: Non Evidenziato

Formattato: Non Evidenziato

difficult to assess experimentally and difficult to anticipate a priori. In fact, macro-molecules Z-potential measured in bulk does not necessarily correspond to the effective charge they bring at the interface. Various methods have been developed to measure interfacial tension, the macroscopic quantity characterizing interfaces, somehow related also to the surface charge.[9]

Optical studies of drop and bubble profiles are extensively applied to study interfaces and their response to surface active molecule uptake.[10,11,12] The shape of drops and bubbles is affected by changes in the surface tension caused by the uptake of surface active molecules at the interface. More recently, dynamic measurements of surface tension have been carried out by several authors.[9,13,14]

These studies are aimed at understanding the mechanisms of transport and insertion of surface-active molecules into void interfaces and/or at investigating the adsorption mechanisms under non-equilibrium conditions (e.g., in systems with periodically varying surface area). The combined knowledge of equilibrium and non-equilibrium effects on adsorption, surface tension and interfacial (visco) elastic properties, shed light on the transfer mechanisms and relaxation effects at the interfaces. Most of these measurements apparata usually employ fast videocamera techniques for recording the time variation of the moving interfaces. Despite the technical progresses and the advanced computational analysis of the images, their ability to measure tiny interfacial oscillation amplitudes is hampered by the relatively low resolution of the classical geometrical optics.

A much deeper insight up to the nanometric scale can be achieved by employing techniques such as the interferometric ones grounded on the undulatory nature of the light. The differential interferometric techniques here applied deeply extend the range of investigable amplitudes from tens of nanometers to the sub-nanometric range.[15,16] The bubble interferometer exploits the analysis of stationary modes of a resonating bubble under small perturbations induced by an external forcing electromagnetic field and allows the study of surface properties with extremely high sensitivity. Importantly, the technique is complementary to the drop/bubble profile methods because, it is sensitive to the charge at the interface.[17] In fact, by applying an e.m. forcing field, the amplitudes of resonant modes depend on interfacial charge. By revealing charge variations, the technique can cover a regime of unusually low surface concentrations, where the adsorbed molecules do not significantly affect the surface tension. Results on air/water interface uptake of

sodium dodecyl sulfate (SDS) were recently presented[18,19] and the technique was extended to oil/water interfaces by investigating oil drops in water.[20]

Indeed, the frequencies of capillary modes depend on bubble geometry, i.e. on its radius and on the constraint of attachment (for tethered bubbles), and are related to the restoring force of surface oscillations, i.e. to the interfacial tension. [21-23] In general for tethered bubbles, the frequencies of the discrete stationary modes, F_l, are expressed by Equations 1a and 1b, given $\omega_{ol} = 2\pi F_l$:

$$\omega_{o1} = \left[\frac{D(a)}{\rho R_o^3} \sigma \right]^{1/2} \qquad \text{for} \quad l=1 \qquad (1a)$$

$$\omega_{ol} = \left[\frac{D(l,a)}{\rho R_o^3} (l+2)(l+1)(l-1)\sigma \right]^{1/2} \qquad \text{for} \quad l>1 \qquad (1b)$$

where σ is the surface tension, ρ the fluid density, R_o the radius of the bubble and *D(l,a)* is a term which depends on the constraint *a* determined by the geometry of attachment.[22-24] In the case of surfactant-covered bubbles (drops), the key parameter is the surface tension σ, which is a decreasing function of the surface coverage by surface active molecules.

Nevertheless, bubble interferometry shows that, for oscillating charged interfaces, the dependence of the resonance frequencies on the charging of the unperturbed interface is nontrivial. This notion was understood by Lord Rayleigh in the prime work on the instability of charged drop dating 1882[25] but a detailed formulation of the theory in the domain of the present applications is still missing.

We present here a study of interfacial properties of small-amplitude fast-oscillating air bubbles in water upon adsorption of soluble proteins. We investigated bovine serum albumin (BSA)[26-27] and lysozyme[28] proteins, chosen to be representative of typical water-soluble globular proteins. Experimental results are presented in sections 3.1. To provide a comprehensive insight into the novelty of the technique, we devoted section 3.2 to study the well-known surfactant SDS. Different theoretical models are developed to derive the dependence of the oscillating bubble resonance parameters, frequency and amplitude, on the adsorption of charged molecules, and are reported in sections 3.3. In Section 3.4 experimental results and theoretical findings are discussed in comparison.

Codice campo modificato

Codice campo modificato

Codice campo modificato

Codice campo modificato

Codice campo modificato

Codice campo modificato

Codice campo modificato

2. MATERIALS AND METHODS

2.1. The bubble interferometric technique. The technique here applied to study interface properties is based on the study of capillary waves rising at the surface of air bubbles when they are perturbed from equilibrium by an external field. In particular, an oscillating electric field is applied in this study. The interferometric method recently developed,[15-19,] is briefly summarized as follows. Bubbles, of the order of 1 mm in diameter, are formed at the top of a stainless-steel hollow electrode protruding out from the bottom of a small square cell and are subsequently captured on a second electrode placed 2 mm over the first one (see Figure 1a). The total cell volume is about 0.5 mL. The bubble radius was measured by means of a CCD camera. Bubble oscillations are excited by a periodic electric field due to the effective net charge existing at the interface, naturally occurring even in pure water. [17, 29]

The amplitude of the exciting force is kept low enough to produce interfacial oscillations in the range of few nanometers. Surface deformation is probed by analyzing the interference of the beams reflected from the bubble, once laser light crosses its diameter. In fact, when traversed by a Gaussian laser beam, the bubble air−water interfaces act as the mirrors of a confocal Fabry−Perot interferometer, due to the difference in refractive indexes. A set of concentric fringes are formed in the backward direction, which depend on the optical path variations of the light inside the bubble when it is deformed by the forcing field. Due to the closed geometry of the bubble only a discrete set of stationary modes, *l*, are excited. The oscillation frequencies slightly deviate from the Rayleigh frequencies of a free bubble[21] due to the attachment of the bubble to a constraint that introduces a new lower frequency mode F_1, that is connected to center-of-mass motion.[22-24] The higher order frequency modes F_l are increased depending on the constraint geometry with respect to free bubble modes. In general, F_l depends on geometry (i.e. the bubble radius and the constraint), and is related to the restoring force of surface oscillations. Several characteristic modes can be observed for millimeter-sized bubbles, with a typical lowest-frequency mode of about 10^2Hz and an amplitude in the nanometer range, well above the ultimate sensitivity of the instrument. In section 3.3 we will report analytical relationships between the oscillating frequencies F_l and the physical properties of a surfactant-covered bubble in terms of the physical properties of the system for different models. At a fixed exciting electric field, the amplitude of surface oscillations (modes) is strictly

connected to the interfacial charge which, in turn, is affected by the absorption of molecular species. Thus, the technique is quite suitable to monitor absorption or desorption of charged molecules in real time by measuring resonance amplitude changes. Figure 1 shows the experimental set up and an example of the resonance spectrum of a bubble in pure water. The inset in Figure 1 b) shows the amplitude increase of the *l=1* mode upon charged surfactant adsorption at the bubble interface.

Lastly, the applied experimental set up is equipped for the on-line measurement of the bulk conductance, enabling a precise monitoring of the molecule concentration in solution.

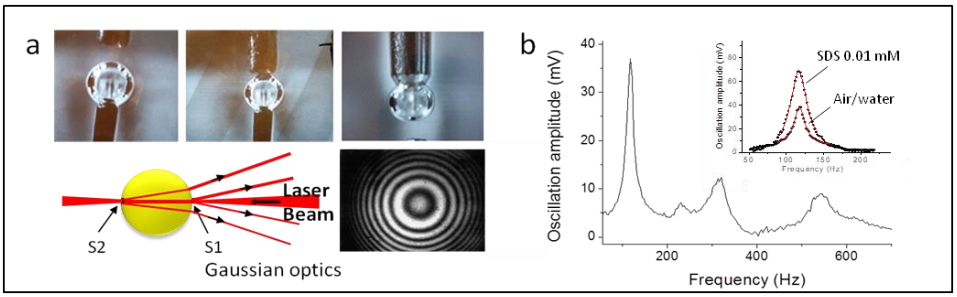

Figure 1. a) The picture shows bubble formation and attachment to the top electrode (top), a drawing of the interfering beams reflected from bubble opposite interfaces S1 and S2 (bottom left) and the concentric fringes of the interference pattern (bottom right). b) Example of the resonance spectrum of pure water. The lowest-frequency peak is the *l* = 1 mode which is the one studied in the experiments. The inset shows the *l* = 1 mode increasing amplitude due to adsorption of SDS at the bubble interface.

2.2. BSA. BSA was purchased from Sigma Aldrich and used without further purification. A stock solution of 2 mg/L ($3.0 \cdot 10^{-8}$ M) in Milli-Q water was prepared.

2.3. Lysozyme. Lysozyme was purchased from Sigma Aldrich and used without further purification. A stock solution of 20 mg/L ($1.39 \cdot 10^{-6}$ M) in Milli-Q water was prepared.

2.4. SDS. High-grade commercial sodium dodecyl sulfate was purchased from Sigma–Aldrich. Experiments were performed applying a freshly prepared stock solution, minimizing the measurement times.

3. RESULTS AND DISCUSSION

3.1 Protein adsorption. We investigated the uptake of BSA and Lysozyme proteins at the air/water interface of millimeter sized bubbles, by monitoring their surface vibration modes in the range of hundred Hertz with sensitivity in the nanometer scale. We focused on conditions of very low degree of surface coverage. Kinetics measurements are targeted to unveil protein adsorption onto the interface including the induction time occurring before surface tension decrease.

3.1.1 BSA Absorption. BSA (molecular weight 66.5 kDa), is a largely studied globular protein. Isoelectric point (IP) and Z-potential of BSA in solution at varying pH, ionic strength and salt are reported in the literature. [30-33] Our measurements are performed at pH= 6.8, for which the Z-potential in bulk is about -20 mV (IP~ 5).[31-33] At the low concentration ($c < 1 \cdot 10^{-8}$ M) and at the pH applied in our study, aggregation process or molecular interaction are not expected. BSA surface activity at the air/water interface has been studied by a variety of techniques under different conditions and, in particular, at low bulk concentration.[34-40] All these investigations indicate that, at low concentrations, the adsorbed molecules mostly maintain their globular conformation without encountering extensive denaturation upon adsorption and that a uniform coating layer of BSA forms.

Interferometric measurements of BSA adsorption were obtained by adding incremental volumes of a few µl of the stock solution to a 450 µl total volume cell filled with pure water. After each addition step, the equilibrium was intended to be reached after the stabilization of the bubble resonance. Figure 2 reports the behavior of the lowest resonant mode showing the resonance frequency (panel a) and amplitude (panel b) versus bulk BSA concentration.

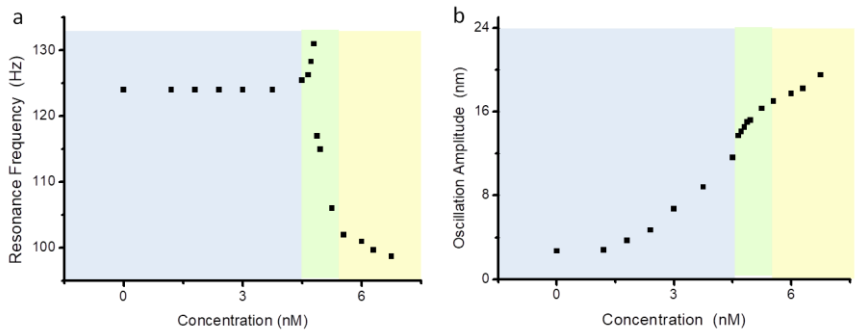

Figure 2. Behavior of resonance frequency (panel a) and amplitude (panel b) at increasing BSA bulk concentration. A 3 volts sinusoidal voltage was applied to the electrodes. The interelectrode distance was 2 mm. The color changes are indicative of the transition-like event and the green strip marks the transition region. Repeated experiments using the same stock solution gave consistent results with a frequency fall of (20 ± 0.5)% and with an amplitude increase by a factor of 4.3 ± 0.2, from the bare bubble to transition. The plotted frequency and amplitude values are obtained as parameters of the resonant-peak fitting to a Lorentzian function.

After the first addition of BSA in solution, an increase in the resonance amplitude was observed without affecting the resonance frequency. This is interpreted as an increase in the interfacial net charge due to protein absorption. A threshold of about 4.5 nM is measured, above which a small increase followed by a deep decrease of the frequency was detected. This behavior was observed for all the shape deformation modes from *l=1* to *l=4*, while a different trend occurs for the radial mode *l=0* as discussed in the next paragraph. Furthermore, the occurrence of this transition-like event in the plot of resonance frequency against concentration in covered bubbles was also observed using a variety of other surfactants, proteins and colloidal suspensions (unpublished data), thus assuming the characteristic of a general phenomenon.

Importantly, the transition was not observed in chloroform-saturated bubbles, a nonpolar molecule (surface tension $\sim 27\ mN/m$ at room temperature). Despite the lowering of the air-water interfacial tension caused by the increased concentration of chloroform at the interface (not necessarily as a monolayer) the lack of a significant variation of the surface potential over a broad range of concentration of

Formattato: Non Evidenziato

apolar molecules like chloroform makes the frequency transition impossible. The explanation for this unconventional behavior in terms of shape instability of charged spherical interfaces will be presented and discussed in the next section 3.3.

The uptake kinetics of BSA can be investigated by creating a bubble in a BSA solution at equilibrium. Figure 3 reports the protein adsorption kinetics obtained for a freshly created bubble in the final 7 nM BSA solution of the previous experiment. The resonance evolution of the new bubble is shown in panel a), where the first measured spectrum resembled that of pure water. The entire transition process was completed in about one hour, as shown in panels b) and c) of Figure 3, where amplitude and frequency are reported as a function of the elapsing time after bubble creation. The relatively slow uptake, lasting more than an hour before reaching an equilibrium condition, makes clear the need of overcoming an energy barrier before getting at the interface, as is typical for soluble proteins that hardly expose their hydrophobic moiety to the external medium.[41]

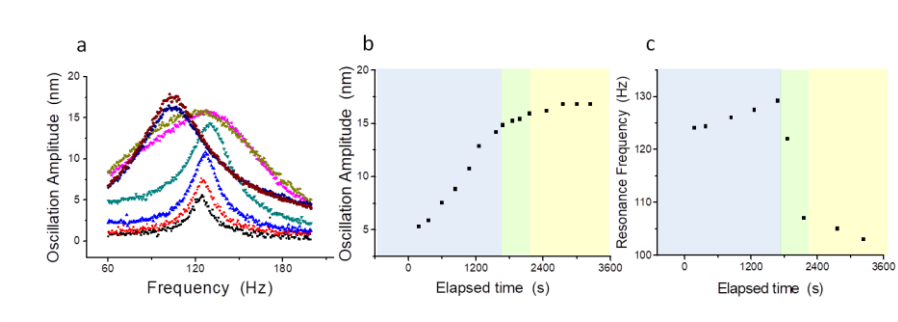

Figure 3. a) Lowest resonance mode evolving during BSA absorption on a just formed bubble in a 7 nM BSA solution; adsorption starts with the lowest amplitude resonance peak at 124 Hz (black spectrum), then causes an amplitude increase (red, blue and green spectra) followed by a transition (pink and olive spectra) to lower frequency resonances ending with the highest peaks at low frequency (navy and brown spectra); b) amplitude evolution; c) frequency evolution. Exciting field and distance between the electrodes was the same as in Figure 2. Color changes are indicative of the transition-like event and the green strip marks the transition region.

Formattato: Non Evidenziato

The evolution of oscillation amplitude indicates a maximum rate of adsorption in the first 1200 s, that lowers for increased surface coverage (Figure 3b).

To complete the exploration of the oscillating bubble behavior during protein adsorption, we dedicated a further experiment to investigate the volume oscillation mode, *l = 0.* Data are shown in Figure 4. Panel a) reports the overall resonance

spectrum of a BSA-covered bubble measured over a wide range of frequencies. In addition to the shape deformation modes at *l = 1, l = 2* and *l = 3* confined in the low-frequency side of the spectrum, we observe the volume mode *l = 0* at frequency above 4000 Hz. It occurs at higher frequencies because for *l = 0* the surface deformation works against both the surface tension and the gas compression inside the bubble. Panel b) shows the resonance frequency of the volume mode with protein bulk concentration. Identical results were found by plotting the eigen-frequency against time. As we can see, no detectable frequency variations are observed, in sharp contrast with the shape deformation modes (*l = 1, 2, …*), reported in Figure 2 for *l = 1*. This is an important experimental finding that will suggest an explanation for this peculiar phenomenology (see section 3.3.4).

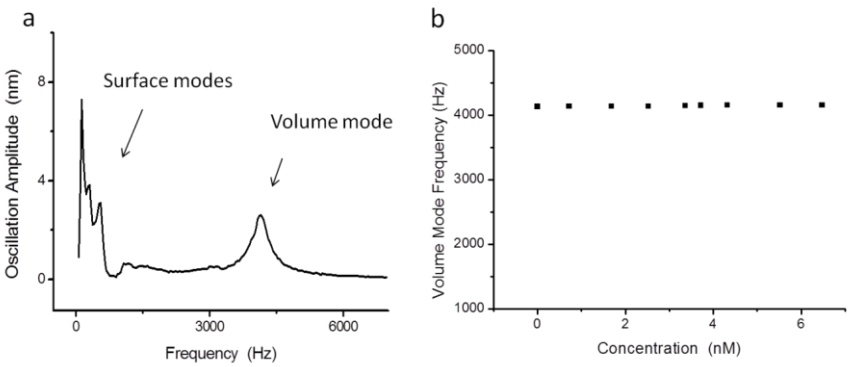

Figure 4. Panel a): Extended resonance spectrum (in the range 0-7000 Hz) of a bubble immersed in a 6.5 nM BSA solution. Surface modes are confined in the lower frequency side of the spectrum while the volume mode *l = 0* stems as a single Lorentzian centered at a much larger frequency, 4200 Hz. Panel b): frequency evolution of the volume mode *l = 0* with BSA concentration. The experiments were performed with acoustic excitation.

3.1.2 Lysozyme adsorption.

The adsorption kinetics of a second well known protein, the lysozyme, was followed. Lysozyme has a molecular weight of 14.4 kDa and an IP slightly above pH 11. We performed the experiment at 40 nM bulk concentration and pH 6.8 where the Z-potential of Lysozyme is about +5 mV.[42] Data in the literature (mainly applying buoyant bubble methods) show that the interfacial properties evolution upon lysozyme adsorption is a slow process, where a first mild effect on surface tension

seen only after few hours, is followed by a final equilibrium hardly reached, even after days.[43-47]

Being mainly interested to unveil the low coverage states, we followed the system during a time interval of 3600 s. Figure 5 reports the results obtained in terms of oscillation amplitude (panel a)) and frequency (panel b)) evolution.

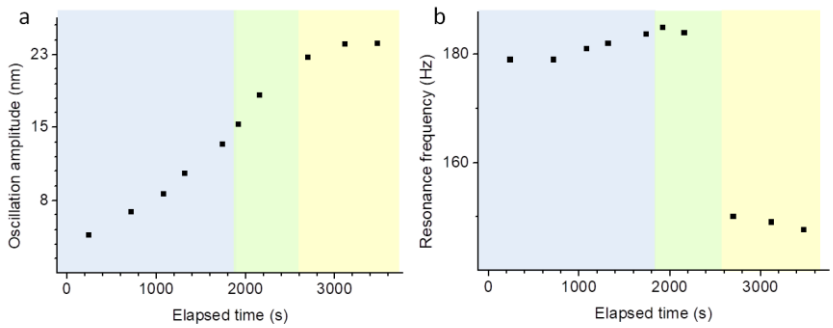

Figure 5. Lowest mode resonance evolving during Lysozyme absorption on a just formed bubble in 40 nM solution; a) amplitude evolution; b) frequency evolution. A 3 volts sinusoidal voltage was applied to the electrodes. The interelectrode distance was 2 mm. The color changes are indicative of the transition-like event and the green strip marks the transition region.

Data show that, similarly to BSA at 7 nM, Lysozyme at 40 nM enters the interface, increases the oscillation amplitude and reaches a transition point in about 30 minutes after bubble creation. Considering the lower molecular weight and the higher concentration with respect to BSA, a higher energy barrier to enter the air/water interface can be involved for the Lysozyme. In fact, adsorption kinetics, besides the diffusion coefficient, is controlled by several factors including hydrophilic/hydrophobic ratio at protein surface and protein deformability. Our results are in agreement with the literature[43-47] and also they satisfy the Traube-rule-like behaviour,[48] an experimentaly-derived rule indicating that the bulk protein molar concentration required to modify the interfacial tension should increase with decreasing the protein molecular weight.

Formattato: Non Evidenziato

In agreement with radio-labelling and fluorescent studies,[46,49] our finding indicate that during the induction time before surface tension decrease, protein concentration at interface increases. Figure 2 a) shows, for BSA, an extended concentration range of almost flat resonance frequencies, measured with a

precision of tenth of Hertz. This argument is in favor of needing a minimal amount of proteins at interface for the onset of a decrease of surface tension.

3.2. SDS Adsorption.

In order to provide a comprehensive set of experimental evidences elucidating the novelty of the technique, we followed the adsorption of SDS surfactant onto the air/water bubble interface. Some results on SDS obtained by the interfeometric technique, have already been presented.[19] SDS is a well-known anionic surfactant that has been extensively investigated.[9,50-56] It is a mild surface-active surfactant with a CMC of about $8 \cdot 10^{-3}$ mol/L. As we are working in water bulk at low surfactant concentration, it is noteworthy to mention that depletion effects are not relevant for SDS, as was recently shown by profile analysis tensiometry.[55]

Here we show data obtained for SDS concentration in the range from 0.0035 to 0.32 mM, with the lowest concentration hundreds times lower than the CMC, with a continuous monitoring of the bulk conductivity upon surfactant addition. After a bubble was created inside the measurement cell and its resonance spectrum was acquired in pure water, SDS was added stepwise. The lowest resonance frequency of the spectrum, reported in Figure 6 a), is constant up to a threshold concentration of about 0.045 mM, where a transition-like event takes place, analogous to that seen for the BSA (Figure 2 a)). Furthermore, Figure 6 b) shows the increase of the oscillation amplitude upon increasing SDS bulk concentration. The first point in concentration was 0.0035 mM, a useless concentration for methods sensitive to variations of the surface tension. In literature, it is reported that concentrations up to 0.3 mM induce changes of surface tension of only few percent with respect to pure water. Thus, the clear frequency variation that we observe in the transition range is not expected to be connected to surface tension variation. Likewise, it can be observed that by further increasing the bulk concentration above the transition, the frequency proceeds with decreasing. If equations 1 a) and b) gave the dependence of the resonance eigen-frequencies on surface tension, a more limited variation would be expected. Data suggest that the reason for the frequency drop and for its further deep decrease should be related to other mechanisms than a σ variation and that a nontrivial dependence of the eigen-frequency of capillary modes on σ needs to be investigated.

Formattato: Non Evidenziato

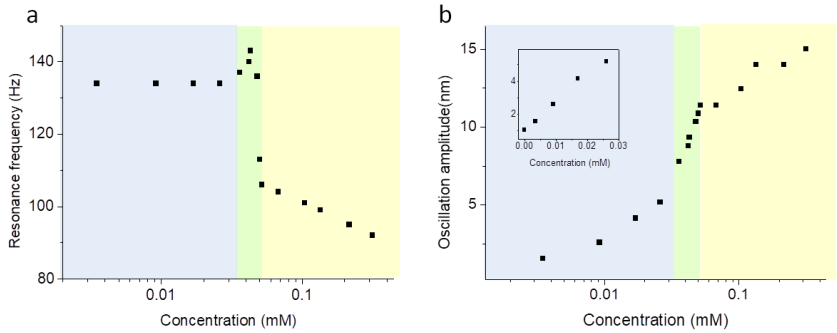

Figure 6. Bubble lowest oscillation mode at varying SDS bulk concentration (logarithmic scale): a) frequency and b) amplitude. The inset reports the lowest concentration points in linear scale. The bubble radius was 0.72 mm and 1 V sinusoidal voltage was applied to the electrodes. The color changes are indicative of the transition-like event.

However, the important point is that, naturally sensing the charge, the technique overcomes the limit of sensitivity associated to changes of σ, giving the opportunity to unveil molecular adsorption by monitoring oscillation amplitudes.

To corroborate the results and to enforce the theoretical understanding of the mechanism underling the nontrivial response of the oscillating bubble upon charge adsorption, we reproduced an analogous investigation of the same system but exciting the bubble by acoustic waves. Cell details and plotting are reported in the supplementary material SM A. Indeed, in perfect agreement with the behavior seen by e.m. excitation, a downward shift of the frequency occurs at 0.045 mM concentration, in correspondence of the transition-like event already observed. This indicates that the transition is a phenomenon not affected by the forcing methods. As recalled above, the characteristics of generality of the behavior and its absence in the case of chloroform adsorption, suggested the involvement of the interfacial charging process in its occurrence.

3.3. Model calculations.

3.3.1. Amplitude of oscillation

Let us focus on the oscillation amplitude of the bubble interface that is sensed up to the sub-nanometric scale by our interferometric technique. In agreement with other authors,[57] we first calculated the equation of motion of an oscillating bubble undergoing shape deformations finding a simple equation for the displacement A_l from equilibrium. We define the deformed radius *R(t)* of the bubble as: $R(t) = R_o + \sum_{l=0}^{\infty} A_l S_l(\theta,\varphi)$, with R_o the unperturbed radius and $A_l S_l(\theta,\varphi)$ the angular deformation profile of the bubble surface developed in spherical harmonics, $S_l(\theta,\varphi)$ of amplitude A_l (see SM B). Following a standard procedure, we write down, in the limit $A_l / R_o << 1$, the equation of motion of the surface deformation:

$$\frac{d^2 A_l}{dt^2} + \gamma_l \frac{dA_l}{dt} + \omega_{0l}^2 A_l = B_l \cos\omega t \qquad (2)$$

where ω_{0l}^2 is the eigen-frequency (proportional to the observed resonance frequency) of a generic *l-th* mode and γ_l is a damping factor related to the medium viscosity. ω and B_l are the angular frequency and the strength of coupling associated to the exciting field-bubble interaction. The validity of the assumption $A_l / R_o << 1$ is verified because A_l falls in the nanometric range while R_o lies in the millimetric range. Hence, anharmonic effects are virtually absent. Equation (2) is nothing but the driven-damped harmonic oscillator equation, the solution of which reads:

$$< A_l^2 > \; = \; \tfrac{1}{2} \frac{B_l^2}{(\omega^2 - \omega_{ol}^2)^2 + \gamma_l \omega^2} \underset{\omega \to \omega_{ol}}{\rightarrow} \frac{B_l^2}{2\gamma_l \omega_{0l}^2} \qquad (3)$$

brackets denoting time average. The oscillation amplitude $(< A_l^2 >)^{1/2}$ linearly depends on the coupling B_l between the charged interface and the applied field. In the case of an electric excitation, the energy of interaction between a charge distribution and the applied potential is given by: $E_{TOT} = q\psi + \mu\nabla\psi + Q\nabla\nabla\psi + ...$ where q, μ and Q are the net charge, the dipole and quadrupole moments generated by the surface charge distribution, ψ is the applied potential and ∇ is the gradient operator. For a homogeneously charged spherical bubble at rest, only the $q\psi$ term survives. Conversely, for an oscillating bubble, the deformation of its surface generates dipole, quadrupole and higher order moments. Thus, B_1 is proportional to the oscillation-induced dipole, B_2 to the induced quadrupole and so on. The calculation of these multipoles is not easy requiring the solution of Laplace's (in

Codice campo modificato
Codice campo modificato
Codice campo modificato
Codice campo modificato
Codice campo modificato
Codice campo modificato
Codice campo modificato

absence of free moving charges) or Poisson's (in the presence of free moving ions) equations for a deformed bubble surface. Attempts have been reported in the literature with regard to drops and bubbles.[58-60] The coupling coefficients B_l are linearly proportional to the bubble surface charge density. Since surface charging essentially arises from protein adsorption, we impose: $B_l \propto \Gamma$, then from eq (2) we find:

Codice campo modificato

$$< A_l^2 >^{1/2} \omega_{ol} \gamma_l^{1/2} = const \cdot \Gamma \qquad (4)$$

Codice campo modificato

That is, the intensity measured at resonance times the resonance frequency is proportional to the amount of adsorbed proteins.

3.3.2. Resonance frequency overview.

Until now, the focus was on the variation of the bubble oscillation. These measurements provide an easy way to monitor variations of the interfacial net charge and hence of any molecular event which determines such variation, like charged protein adsorption and desorption and the interaction of the adsorbed layer with other charged species present in the surrounding solution. Indeed, as we will detail shortly, the bubble eigen-frequencies, are strongly affected by surface charges too. The experimental results are rather puzzling, especially the sharp fall in the eigen-frequencies observed at certain critical concentrations of added proteins. We tackled the problem from different points of view. In section 3.3.3 we draw a relationship between the eigen-frequencies and the surface tension for an oscillating bubble. Details are reported in SM B. Next, we relate the variation of the surface tension with the concentration of surface-active molecules by a standard approach, showing that the fall of the frequencies is consistent with a picture of strong and favorable adsorbate-adsorbate interactions. However, we will show later that this model is inconsistent both with the data on the oscillation amplitudes, and with the expected values of surface tension of protein monolayers taken from the literature. In section 3.3.4 we propose a different model based on the Rayleigh instability of oscillating charged globules. To do this, we need to revise the notion of surface tension for systems both charged and dynamically deformed. Most of the mathematics is contained in SM C. Finally, in section 3.3.5 and SM D we investigate

the time evolution of protein adsorption as measured through the variation of the oscillation eigen-frequencies.

3.3.3. Resonance bubble oscillations and models of surface coverage at equilibrium (strong interactions model).

The calculation of the eigen-frequencies of a surfactants-covered bubble is performed starting from the usual Navier-Stokes equations. Even in the linearized approximation (valid for small oscillation amplitudes), considerable intricacies arise. Conversely, the theory becomes transparent by using purely irrotational approaches that disregard rotational (viscous) motions. These models produce excellent numerical results when compared with–Navier-Stokes based approaches.[61] An overview of the calculations is given in SM B. In eqs (1 a,b) we already reported the final formulas for the bubble eigen-frequencies F_l ($\omega_{ol} = 2\pi F_l$) relative to the *l-th* shape deformation mode.

Classical equilibrium approach. We first calculate the surface coverage Γ through a standard minimization procedure of the total energy of the system (bulk + interface) as shown in SM B. We obtain a non-linear relationship between Γ and the dimensionless surfactant bulk concentration $\overline{C}$ [62]

$$\frac{\Gamma/\Gamma_{\max}}{1-\Gamma/\Gamma_{\max}}\exp\left(-\frac{2\beta}{k_B T}\frac{\Gamma}{\Gamma_{\max}}+\frac{Z_+ e}{k_B T}\Phi\big|_R\right)=K\overline{C} \qquad (5)$$

where k_B is the Boltzmann constant, T the absolute temperature, $\Gamma_{\max}$ is the maximum allowed coverage, K is the binding constant of the surface-active molecule (protein) to the interface and the parameter β accounts for the intermolecular interactions among the adsorbed surface-active. Lastly, the term $Z_+ e\Phi\big|_R$ (with Z_+ the number of net charges of the protein, e the electron charge and $\Phi\big|_R = \Phi(\Gamma)\big|_R$ is the electrostatic potential calculated at the interface R. It describes non-local effects of the adsorbates through long-range electrostatic forces. Equation (5) is the Davies isotherm, reducing to the Frumkin isotherm[63] in the limit $\Phi\big|_R \to 0$. The above arguments apply to equilibrium interfaces alone. Inserting eq (5) into the expression for the total free energy, we find in SM C a compact expression for the interfacial tension. Although more refined theories are present in the literature, the formula we derived is more suitable to tackle the complex problem of deformed interfaces,

Codice campo modificato
Codice campo modificato
Codice campo modificato
Codice campo modificato
Codice campo modificato
Codice campo modificato
Codice campo modificato
Codice campo modificato
Codice campo modificato

which is the ultimate goal of our study. In the limit of small surface potentials (the Debye-Huckel limit) we calculated for an *un-deformed* sphere:

$$\sigma_{udeformed} = \sigma_o + k_B T \Gamma_{\max} \log\left(1 - \frac{\Gamma}{\Gamma_{\max}}\right) + \Gamma_{\max}\beta\left(\frac{\Gamma}{\Gamma_{\max}}\right)^2 - \frac{(Z_+ e\Gamma)^2}{2\varepsilon\kappa} \qquad (6)$$

where σ_o is the interfacial tension of pure solvent (water), κ is the inverse of the Debye length and ε the dielectric permittivity. Inserting eq (6) into eqs (1 a,b) and relating Γ to $\bar{C}$ by eq (5), we find the searched relationship between the eigen-frequencies ω_{ol} and the bulk surfactant concentration $\bar{C}$.

Such a naïve model reproduces some of the experimental findings. Indeed, as shown in the SM D, the plot of Γ against $\bar{C}$ (eq (5)) shows a first-order discontinuity, provided β is above a critical value. That is, strong attractive short-range interactions among proteins lead to clustering. In turn, according to eq (6), this produces a fall in the surface tension and then a lowering of the resonance frequencies (eqs (1)).

Albeit reasonable, this model does not reproduce the smooth variation of the oscillation amplitudes with concentration or time observed experimentally. Indeed, such a phase transition should give up also with a jump in the surface coverage (see SM D) and hence a jump of the amplitude.

Consequently, we look for a different dynamic theory. The above arguments strictly apply to equilibrium interfaces alone, while our measurement apparatus is inherently a non-equilibrium one. We will see in section 3.3.4 that, in presence of surface charges, the restoring force, which determines the surface mode frequencies of bubbles cannot be directly compared with the surface tension measured with static or quasi-static techniques.

3.3.4 "Apparent" surface tension in oscillating systems (shape transition model).

The implicit assumption made in the previous section is to assume a homogeneous surface tension in any region of the bubble interface. Such an assumption is certainly true for a surface at rest or for oscillations that preserve the spherical symmetry (known as "breathing" or volume modes with *l = 0*), but it becomes questionable when considering surfaces undergoing less symmetric deformations

Codice campo modificato
Codice campo modificato
Codice campo modificato
Codice campo modificato
Codice campo modificato
Codice campo modificato
Codice campo modificato
Codice campo modificato
Codice campo modificato
Codice campo modificato

(*shape* oscillations). Shape oscillations increase the mean surface area with respect to a bubble at rest. In addition, they give rise to regions of different local curvature over the bubble surface. While a variation of surface area associated to radial expansion/compression of drops or bubbles is commonly used to measure static surface tension by the Young-Laplace equation (or, in the case of periodic variations, to investigate the so-called dilatational rheology of monolayers[64]), more intriguing is the onset of regions with different curvatures during shape oscillations. As a matter of fact, long-range repulsive forces among the adsorbates (proteins) stabilize regions of greater curvature where, eventually, charged particles accumulate (a well-known effect in electrostatics, theoretically[65,66] and experimentally[67,68] proven).

Long time ago, Lord Rayleigh[25] foresaw that in a charged and conducting fluid globule undergoing *shape* oscillations, the eigen-frequencies occurred always at *lower* values than in uncharged globules. This behavior arises from the combined effect of the surface tension, which tends to maintain the drop (bubble) shape spherical, and the electrostatic repulsion from the charges, which tends to tear the drop (bubble) apart. The eigen-frequency decreases with the square of the fluid electric charge, tending to zero when the surface tension is exactly balanced by the electrostatic repulsion. When this critical condition has been reached, the system evolves toward a less symmetric equilibrium state where the minimum energy configuration is given by the ellipsoidal instead of the spherical shape. This sort of sphere-to-ellipsoid transition has been investigated in different physical systems[69-71] and falls in the broader field of the "buckling transitions", widely studied in the engineering literature. On further charging the fluid globule, it breaks-up into smaller droplets[72]. Such an instability phenomenon inspired early models of nuclear fission[73] and it is currently used in a lot of technological applications (for instance, the electro-spray technique[74] and its applications in Mass Spectrometry.[75,76] A similar behavior is found when considering elastic forces instead of surface tension forces (the classical problem of non-spherical shapes in charged membranes[77]). Despite our system, constituted by an oscillating gas bubble covered by charged proteins, is different from that investigated by Rayleigh, the two problems share striking similarities and lead to qualitatively similar conclusions.

A simple model for the calculation of the 'apparent' surface tension σ_{app} of an oscillating bubble is shown in SM C. In the essence, the surface tension σ of a charge-bearing deformed sphere in contact with an electrolyte solution reads:

Codice campo modificato

Codice campo modificato

$$\sigma \approx \sigma_{undeformed} - \frac{(Z_+ e\Gamma)^2}{2\varepsilon}\zeta \qquad (7)$$

The first term, $\sigma_{undeformed}$, is the surface tension of the un-deformed sphere given by eq (6) while the second term describes the variation of the electrostatic effects due to the local deformation ζ. This latter term is present in drops/bubbles undergoing shape oscillations alone, while it disappears in the case of a regular sphere, either at rest or undergoing radial oscillations (*l = 0* mode). It is worth noting that the surface tension σ of a deformed sphere is no longer constant but follows the deformations of the interface (ζ depends on the polar angles ϑ and ϕ). This term has a deep influence on the eigen-frequencies of a charged sphere. As shown in SM C, the frequency of a generic *l-th* shape deformation behaves as:

$$\omega_{ol} \approx \left[\frac{D(l,a)}{\rho R_o^3}(l+2)(l+1)(l-1)\left(\sigma_{undeformed} - \frac{(Z_+ e\Gamma)^2}{(l+2)(l-1)\varepsilon}R_o\right)\right]^{1/2}$$

$$\equiv \left[\frac{D(l,a)}{\rho R_o^3}(l+2)(l+1)(l-1)\sigma_{app}\right]^{1/2} \qquad l \geq 2 \qquad (8a)$$

the "apparent" surface tension being defined as: $\sigma_{app} \equiv \left(\sigma_{undeformed} - \frac{(Z_+ e\Gamma)^2}{(l+2)(l-1)\varepsilon}R_o\right)$.

Equation (8a) evidences a fall in the eigen-frequency ω_{ol} of the *l-th* mode on increasing the surface charge density $Z_+ e\Gamma$. When charging effects overcome the surface tension $\sigma_{undeformed}$ (eq (6)), a sudden transition to an elliptically shaped bubble takes place (see SM E). The oscillations about the new equilibrium shape occur at different frequencies. Our linearized model cannot predict geometry and frequencies of the new equilibrium state, they can be calculated only by including non-linear terms in the surface deformation.

Although the effects of the electrostatics on the static surface tension $\sigma_{undeformed}$ (eq (6)) and on the shape oscillation frequencies ω_{ol} (eq (8a)) are similar, their magnitude is markedly different. Using the experimental bubble radii (less than 10^{-3} *m*), the Debye length in pure water (where $H^+ = OH^- = 10^{-7}$ *moles liter*$^{-1}$) and setting *l = 2*, we estimated that the variation of the oscillation frequency for a shape deformation mode is as high as 10^2-10^3 times the variation of the static surface tension (see SM E). Similar results hold when we compare shape ($\boldsymbol{l \neq 0}$) and radial (

Codice campo modificato
Codice campo modificato
Codice campo modificato
Codice campo modificato
Codice campo modificato
Codice campo modificato
Codice campo modificato
Codice campo modificato
Codice campo modificato
Codice campo modificato
Codice campo modificato
Codice campo modificato
Codice campo modificato
Codice campo modificato
Codice campo modificato
Codice campo modificato
Codice campo modificato
Codice campo modificato

$l = 0$) oscillations. Radial oscillations are much less sensitive to surface charging than shape oscillations, the electrostatic effects being contained in the small term $\sigma_{undeformed}$ alone defined by eq (6). Neglecting anchoring effects, one obtains for the radial mode[62] :

$$\omega_{oo} \approx \left[\frac{1}{\rho}\left(\frac{3\gamma}{R_o^2} P_o + \frac{2\sigma_{undeformed}}{R_o^3}(3\gamma - 1) \right) \right]^{1/2} \qquad (8b)$$

where γ is the polytropic exponent ($\gamma \approx 1.4$ for air) and P_o is the external pressure.

These results suggest that the fall of the resonance frequencies of the *shape* vibrational modes alone can be used as a sensitive tool to monitor surface charging even at very low concentration.

A word of caution is in order. In deriving eq (8a) we assumed that the charge density (proportional to the protein surface excess Γ) remains constant during the time-dependent shape deformation of the spherical interface. As a consequence, a variation of the potential is due to the deformation of the interface alone. This is correct for fast interfacial deformations—because adsorbed molecules cannot migrate toward more favorable positions. Different figures arise by allowing protein redistribution. This latter case is expected to hold for slow motions of the interface and/or fast migration rates of the adsorbates. The real situation probably lies in between these limiting cases. In our experiments, bubbles oscillate in the range of 10^2 Hz (the region of bubble resonance) enabling for a small polarization in the protein surface density during the oscillation cycle. By investigating the dependence of the oscillation amplitudes on the intensity of the electric field, as shown in SM F, we confirmed the hypothesis of small polarization.

Independently of the exact estimate of the surface charge density and surface potential, our model predicts a very different behavior of the eigen-frequencies depending on the kind of surface deformation.

3.3.5 Time evolution of the bubble eigen–frequencies: adsorption kinetics.

The experimental kinetics reported above for BSA and Lysozyme (Figures 3 and 5) significantly deviate from the ideal behavior predicted by a sequential binding

Codice campo modificato
Codice campo modificato
Codice campo modificato
Codice campo modificato
Codice campo modificato
Codice campo modificato
Codice campo modificato
Codice campo modificato

kinetics. If we assume that proteins are diffusively transported from the bulk phase to the bubble interface and neglect curvature effects owing to the large radius of the bubble,[78] we would expect a very fast kinetics, a prediction in contrast with the experimental findings, both from the literature and from our results.

To rationalize the experimental data, we employed an advanced version of the classical Ward and Tordai model[79] widely employed to describe diffusion-controlled adsorption kinetics. Specifically, we used an equation developed by Liggieri et al.[80]

$$\int_0^{\Gamma(t)} \frac{d\Gamma'}{g(\Gamma')} = \sqrt{\frac{D_{eff}}{\pi}} \left[2\bar{C}\sqrt{t} - \int_0^t \frac{C(\tau)}{\sqrt{t-\tau}} d\tau \right] \qquad (9)$$

where $\Gamma(t)/\Gamma_{max}$ is the fraction of the interface covered by proteins, $\bar{C}$ is the dimensionless diffusant concentration in the bulk phase, $C(\tau)$ its concentration calculated within a tiny layer beneath the interface (the sub-phase) and τ is a dummy time variable of integration ranging from 0 to *t*. $g(\Gamma')$ accounts for the coverage-depending part of the adsorption rate ($g(\Gamma') = 1 - \Gamma'/\Gamma_{max}$ that is, the available sites of surface binding decrease at increasing coverage). Lastly, D_{eff} (s^{-1}), is a scaled effective diffusion coefficient, $D_{eff} = D\Gamma_{max}\exp(-\Delta E/k_B T)$, modulated by an energy barrier ΔE for the entry of the protein inside the interfacial region. In order to solve the integral equation (9) we have to express $C(\tau)$ as a function of $\Gamma(\tau)$ by assuming a local equilibrium between the sub-phase and the interface concentrations. In the simplest approximation, we consider a linear relationship: $\Gamma/\Gamma_{max} \approx KC$ (Henry law), where *K* is the dimensionless binding constant of the diffusant to the interface. Such a relationship has been proved to be a good approximation in the limit of small $\Gamma(\tau)$ yielding from eq (9):

$$\frac{\Gamma(t)}{\Gamma_{max}} = K\bar{C}\left[1 - \exp\left(\frac{D_{eff}t}{K^2}\right) \cdot erfc\left(\sqrt{\frac{D_{eff}t}{K^2}}\right)\right] \qquad (10)$$

erfc(x) being the complementary error function.[81] Asymptotics to eq (10) are:

$$\Gamma(t) \approx 2\bar{C}\Gamma_{max}\sqrt{\frac{D_{eff}t}{\pi}} \qquad t \to 0 \qquad (11a)$$

Codice campo modificato

Codice campo modificato

Codice campo modificato

Codice campo modificato

Codice campo modificato

Codice campo modificato

Codice campo modificato

Codice campo modificato

$$\Gamma(t) \approx \Gamma_{\max} K\overline{C} \qquad t \to \infty \qquad (11b)$$

Once the interfacial excess $\Gamma(t)$ has been estimated by eqs (11), we insert it into the formulas for the surface tension, eq (6), and, through eqs (1), eventually we find a relationship between the bubble oscillation eigen-frequencies ω_{ol}^2 and time:

$$\omega_{ol}^2 \approx \omega_{ol}^2\Big|_{\Gamma=0} - const \cdot \sqrt{t} \qquad \text{small } t \qquad (12)$$

where $\omega_{ol}^2\Big|_{\Gamma=0}$ is the eigen-frequency of the bare bubble ($\Gamma = 0$) while the multiplicative constant turns out to be: $const \equiv 2\overline{C}\Gamma_{\max}\sqrt{\frac{D_{eff}}{\pi}} k_B T D(l,a) \frac{(l-1)(l+1)(l+2)}{\rho R_0^3}$ (when *l=1* the function $D(l,a)\frac{(l-1)(l+1)(l+2)}{\rho R_0^3}$ must be replaced by $D(a)\frac{1}{\rho R_0^3}$, see eqs (1)). On the contrary, in the limit $t \to \infty$, the resonance frequency ω_{ol}^2 tends to a constant value. In practice, eq (12) applies only to extremely dilute solutions and low surface coverage. A more correct behavior is developed in SM D in the opposite high coverage limit.

The main result is that the binding kinetics strongly depends on the chemical structure of the proteins. Experimentally, BSA adsorption kinetics goes to completion within hours at 7 nM concentration (Figure 3), while Lysozyme follows similar rate of adsorption as BSA but at much higher concentration of 40 nM (Figure 5).

Moreover, looking at Figure 3b and 5b, the time decay of the bubble oscillation frequency is much more rapid and non-linear than the one predicted by eq (12). Again, we could invoke a transition-like behavior of the adsorbed protein monolayer once a critical concentration has been reached as modeled in SM D. But, as it will be discussed in section 3.4, this picture is rather unrealistic because it requires strong protein-protein interactions. A more likely explanation is related to the charge-dependent behavior of the eigen-frequencies described by eq (8a) showing a sharp decrease of the resonance frequency with the coverage.

3.4. Theoretical results and their comparison with the experimental findings.

Codice campo modificato
Codice campo modificato
Codice campo modificato
Codice campo modificato
Codice campo modificato
Codice campo modificato
Codice campo modificato

Our technique is inherently transparent because it works in the realm of the harmonic oscillations. Indeed, oscillation amplitudes are in the nanometer range, in comparison with the millimeter size of the bubble diameter. In spite of this advantage, a full understanding of the physics behind adsorption processes is far to be reached. Adsorption kinetics strongly depend on protein bulk concentration, its diffusion coefficient and, more important, on the work required to accommodate themselves at the interface. After a considerably long lag time where slope variations are small, there is a sharp drop in the plot of the resonant frequency of oscillation vs. time (see Figures 3 and 5). This rapid fall is related to the variation of the "apparent" surface tension with protein surface coverage Γ (see Figures 2). Analogous rapid fall is observed for SDS at varying concentration (see Figure 6). The flatness of the oscillation frequency before the transition and the following sharp decay after the transition can be explained in two alternative ways. The first one is a classic gas-to-liquid transition model as described by a simple equilibrium model developed in section 3.3.3. To be valid, it requires that the protein-protein (surfactant-surfactant) interaction parameter β is above a critical threshold β_{crit} (see SM D). This model can be addressed as a 'strong interactions' model.

Codice campo modificato

Codice campo modificato

We developed a second different model inspired by the classical paper of Rayleigh on the *shape* oscillations of charged fluid globules[25] This model can be addressed to as 'shape transition' model. As discussed in section 3.3.4, the electrostatic repulsion stabilizes elongated shapes, while the interfacial tension at the bubble-fluid interface favors the spherical shape. Consequently, the eigen-frequencies associated to shape deformation modes should rapidly decrease on charging the bubble surface. Some numerics are reported in SM E. Distinctively, this frequency lowering was predicted to be negligible for volume oscillations (the radial symmetric mode $l = 0$) as shown by comparing eqs (8a) and (8b). Experiments do confirm our hypotheses. Indeed, the comparison of Figure 2 with Figure 4 highlights the different behavior of the eigen-frequencies for shape and volume oscillations on varying the protein bulk concentration. The same is valid for SDS (data not shown).

It is worth saying that the ultimate explanation for the anomalous (and potentially useful) fall of the "apparent" (i.e., deduced by the frequency, eqs (1)) surface tension resides in the intrinsically dynamic nature of the interface.

Lastly, the behavior of the amplitudes of the interfacial oscillations is interesting. At variance of the resonance frequencies discussed in figures 2 a) and 6 a), which

shows a first-order transition for some critical concentrations, the oscillation amplitude reported in figures 2 b) for BSA and in Figure 6 b) for SDS show a smooth behavior with a hardly detectable discontinuity.

At this point, the two models are worth comparing. The first model (strong interactions model) invokes a cooperative adsorption due to strong protein-protein interactions. This assumption turns out to be wrong. Indeed: A) Surface tension data reported in the literature obtained by various static and dynamic techniques, do not evidence any sharp behavior at low concentration. Moreover, beside the fall at the transition, a higher rate of frequency variation, than predicted from eq (1), is seen after the transition (with potentially useful sensitivity increase). This is evident for example for SDS above the transition, showing a deeper variation of ω_{ol}, than usually expected (eq (1)) for the low *c* range (0.05 - 0.3 mM (see Figure 6 a)). Following the shape transition model (eq (8)), frequency are diminished with respect to simple $\sigma_{undeformed}$ dependence by the second, charge dependent term.

Codice campo modificato

Codice campo modificato

B) According to eq (4), the product of the peak intensity at resonance times the resonance frequency, times the square root of Full Width at Half Maximum (FWHM), must be proportional to the surface coverage Γ. If the sharp transition is interpreted following the strong interaction model, a sudden increase of the interfacial coverage beyond a critical surfactant concentration would predict a similar sharp increase of the amplitude (because of the rising of surface charges). So, as shown in SM D, Γ should exhibit a first-order phase transition. On the contrary, experimental data yield smooth curves, as shown in Figure 7, ruling out the occurrence of protein cooperative effects in the concentration range involving the transition-like event.

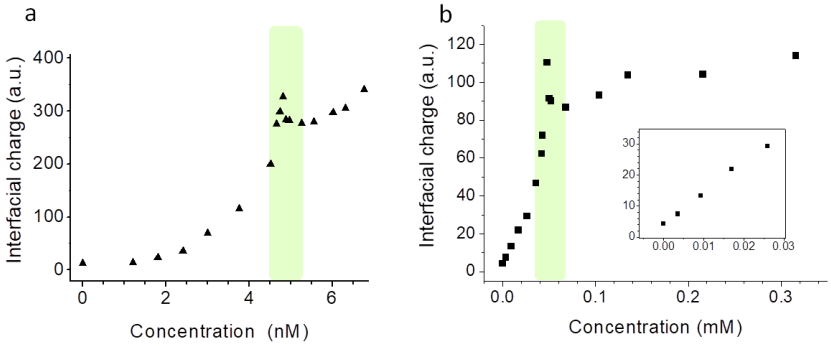

Figure 7. Behavior of the product (amplitude)x(frequency)x(FWHM$^{1/2}$) of the resonance peak, indicated as interfacial charge (arbitrary units), against bulk concentration. a) BSA and b) SDS; the inset enlarges the lower concentrations. Disregarding the small peak at the transition, here highlighted in green, the quantity (amplitude)x(frequency)x(FWHM$^{1/2}$) behaves as a typical second-order transition.

The second model, presented in section 3.3.4 (the shape transition model), accounts for the sharp decrease of the resonance frequency by considering a bubble transition towards an elliptic-shaped equilibrium upon charged protein adsorption. This effect is due to a change of the restoring-force balance between surface tension and charge repulsion inside the bubble (Rayleigh instability). This mechanism does not require a sharp increase of the surface coverage Γ, yielding, at most, a small variation in the slope because of the bubble geometrical changes (second-order phase transition). Unfortunately, the exact shape of the deformed bubble and its oscillation frequencies cannot be predicted by our linear theory. What we can say at moment is that, beyond a critical charge, the spherical shape becomes unstable.

Although the most prominent experimental findings were reasonably understood by the shape transition model, there are some features that deserve further investigations. We observed a puzzling small peak (overshoot) just before the fall of the resonance frequency (Figures 2,3,5,6). This peak was observed both in equilibrium condition (by varying the protein concentration) and in 'dynamic' (by varying time) experiments. This observation rules out the possibility that overshoots are due to protein relaxation (e.g., denaturation) upon adsorption, a phenomenon often found in protein adsorption kinetics.[82-84] The physical meaning of the overshoot remains at the moment elusive.

We note that, within the approximation of eq (4), the data plotted in figure 7 are proportional to the effective charge of the bubble at varying protein/surfactant bulk concentration, and hence to the surface coverage Γ(C). The interfacial charge can be estimated as a ratio to the value found for the same bubble in pure water (uncovered). Literature data report a wide range of Z-potential values for the air/water interface, corresponding to a charge density lying in the range 10^{-5}–10^{-4} C/m^2, of negative sign.[29,85-87] In a previous work[17] a charge density of 1.8 10^{-5} C/m^2, independent of bubble radius, was obtained for air bubbles in water via the interferometric technique. Accordingly, we can evaluate the effective charge density of a coated bubble and discuss the results in terms of the surface coverage Γ, comparing them with literature data obtained by model isotherms.

In the case of BSA (Figure 7a)), no linear behavior of charge (protein) uptake is seen, not even in the lowest concentration interval. The charge density obtained at 7 nM (0.46 mg/L) bulk concentration, the highest concentration investigated, is about 20 times that of pure water. Despite the difficulty in estimating the charge-per-protein ratio (Zp) of interfacial BSA, data from vibrational sum-frequency generation and ellipsometry,[33] showing a conserved isoelectric point of BSA at air/water interface with respect to the bulk, allow us to estimate Γ(C) using bulk values of Zp. In fact, assuming Zp ≈ 5,[30,88] we calculate the amount of adsorbed proteins at 7 nM to be in the range of $\Gamma \approx 6\cdot10^{-10} - 6\cdot10^{-9}$ mol/m^2, depending on the charge density used for the bare bubble (see above). These figures are in agreement with the literature. Cho et al. found $\Gamma \approx 7\cdot10^{-9} - 1.5\cdot10^{-8}$ mol/m^2 for BSA bulk concentration of 1 - 10 mg/L (i.e. 15 nM – 150 nM),[89] while at higher concentration, 40 mg/L, the coverage was evaluated as $3.7\cdot10^{-8}$ mol/m^2 by ellipsometry.[40]

Charge increase due to SDS adsorption (Figure 7 b)) behaves linearly in the low concentration range (from 0 to 0.04 mM), in agreement with Henry's law. In this region, the bubble charge increases, being three times that of the bare bubble at 0.01 mM. Electrophoretic mobility measurements on nanobubbles in SDS solutions reported similar behavior, measuring a Z-potential variation from -20 mV in pure water to -40 mV in 0.01 mM SDS,[90] followed by a smoother increase in the Z-potential at higher concentrations. Again, we can thrust the experimental findings to a comparison with estimations in the literature by phenomenological isotherm models, suggesting surface charge $\Gamma \approx 1\cdot10^{-7} - 3\cdot10^{-7}$ mol/m^2 at 0.1 – 0.2 mM bulk concentrations.[56] Such values are compatible with our evaluation that, by arbitrarily hypothesizing a 30% ionization degree of SDS at the interface,[56] indicates a surface

coverage of $\Gamma \approx 2 \cdot 10^{-8} - 1 \cdot 10^{-7}$ mol/m^2 (depending on the value given to the air/water interface charge). Importantly, we recall that the investigated concentration range covers the induction time and the very beginning of the adsorption isotherm, where the surface tension is only slightly affected by surface active molecules, in agreement with the litterature.[54]

4. CONCLUSIONS

The oscillating bubble interferometric technique is apt to follow the charge uptake by the interface with excellent sensitivity. Variation of the electrostatic surface potential modifies both the oscillation frequencies at resonance (through a Rayleigh-type instability mechanism) and the oscillation amplitudes (through a surface charge-electric field coupling). The first important consequence is that the technique has been demonstrated to be among the very few monitoring surface charge alterations. Protein/surfactant uptake modifies the charge in a concentration dependent manner. As a consequence, if one knows the molar charge, an estimation of the surface coverage can be done without any modelling, especially at low concentrations.

On the other hand, depending on the degree of coverage and on protein/surfactant specificity, adsorption may involve rearrangements of the water molecules of the interfacial layer, modulating the effective charging.[91,33] To this respect the bubble interferometer, applied in solutions at varying pH, ionic strength, or in the presence of more than one surface-active molecule, can represent a powerful tool of investigation. In fact, despite absolute quantifications can be difficult and model dependent, to obtain high sensitivity on surface charge variations is quite a desirable feature in many experimental situations.

The technique may be of major relevance in the perspective of future applications in biology. In fact, it represents a promising methodology for in vitro investigation of protein coated surfaces, to which charge variations are induced by the interaction with the controlled surrounding bulk environment. In this scenario, it is worth noting that a very low amount of protein (in the order of nanomoles) is needed and this potentially opens to the possibility to study highly relevant proteins, for which a limiting step is the yield of production and purification.[92] In fact, other technologies

developed for studying receptor-ligand interactions[93,94] normally require a large amount of material, in the µM to mM range, often only obtained for protein isolated domains,[95,96] thus limiting the global understanding of the receptor-ligand interaction.

Formattato: Non Evidenziato

It is worth to underline that also the transition-like fall of the resonance frequency, observed once a large enough charge surface concentration has been reached, is the other face of the same coin. Although, a complete interpretation is still missing, the strongly non linear behaviour of the frequency against the surface charge, may offer an excellent expansion of sensitivity in this concentration region.

Moreover, we recall that the same technique can be developed to follow the charge properties of drops in water upon loading of very low amount of proteins or other surface-active molecules or combinations of them thus profitably following kinetics. This can be an interesting outlook in technological applications involving foam and emulsion stabilization issues.[97]

AUTHOR INFORMATION

Corresponding Author

*E-mail: paola.brocca@unimi.it

*E-mail: araudino@dipchi.unict.it

Notes

The authors declare no competing financial interest

ACKNOWLEDGMENTS

A.R. thanks the University of Catania (Progetto di Ateneo 2016-2018) for partial financial support. P.B. thanks the BioMeTra Dept of the University of Milano for partial financial support (PSR2018 grant). Authors like to thank Profs Laura Cantù and Anna Moroni for interesting discussions.

KEY WORDS

Oscillating bubble, interfacial charge, surface charge, interfacial tension, surface tension, surface pressure, capillary waves, small oscillation amplitude, nanometer range oscillations.

REFERENCES

(1) Narsimhan, G.; Xiang, N. Role of Proteins on Formation, Drainage, and Stability of Liquid Food Foams. *Annu Rev Food Sci Technol*. **2018**, 9, 45-63.

(2) Glaser, L. A.; Paulson, A. T.; Speers, R. A.; Yada, R. Y.; Rousseau, D. Foaming behavior of mixed bovine serum albumin−protamine systems. *Food Hydrocolloids* **2007**,21, 495−506.

(3) Zhao Y.; Jones S. A.; Brown M. B. Dynamic foams in topical drug delivery. *J Pharm Pharmacol*. **2010** 62, 678-84.

(4) Serrano, A. G.; Pérez-Gil, J. Protein–lipid interactions and surface activity in the pulmonary surfactant system. *Chem Phys Lipids*, **2006,** 141, 105-118

(5) Langevin, D. DNA Interactions with Polymers and Surfactants, Chapter 10 Dias R.S.; Lindman B. editors, Wiley, **2008**

(6) Zaitsev, S. Dynamic surface tension measurements as general approach to the analysis of animal blood plasma and serum. *Adv Colloid Interface Sci.* **2016**, 235, 201–13.

(7) Jang, H.; Rusconi, R.; Stocker, R. Biofilm disruption by an air bubble reveals heterogeneous age dependent detachment patterns dictated by initial extracellular matrix distribution. *npj Biofilms and Microbiomes* **2017** 3, 6

(8) Boni L.; Fuller G.G.; Inglis R.F.; Fischer P. In-Situ Quantification of the Interfacial Rheological Response of Bacterial Biofilms to Environmental Stimuli. **2013,** *PLoS ONE* 8, e78524.

(9) Miller, R.; Liggieri, L. editors. Bubble and drop interfaces. Progress in colloid and interface science Leiden: Brill Publ; **2011**.

(10) Miller, R.; Fainerman, V. B.; Makievski, A. V.; Leser, M.; Michel, M.; Aksenenko, E. V. Determination of protein adsorption by comparative drop and bubble profile analysis tensiometry. *Colloids Surf B.* **2004**, 36,123–6.

(11) Berry, J. D.; Neeson, M. J.; Dagastine, R. R.; D. Y.C. Chan, Tabor, R. F. Measurement of surface and interfacial tension using pendant drop tensiometry. *J. Colloid Interface Sci.* **2015**, 454, 226–237.

Formattato: Non Evidenziato

(12) Kairaliyeva, T., Aksenenko, E. V., Mucic, N., Makievski, A. V., Fainerman, V.B., Miller, R. Surface tension and adsorption studies by drop profile analysis tensiometry, *J. Surfact. Deterg.* **2017**, 20, 1225-1241.

(13) Noskov, B. A.; Mikhailovskaya, A. A.; Lin, S.-Y.; Loglio, G.; Miller, R. Dynamic Surface Properties of Poly(N-isopropylacrylamide) Solutions. *Langmuir* **2010**, 26, 17225–1723.

(14) Miller R., Aksenenko E. V., Fainerman V. B. Dynamic interfacial tension of surfactant solutions *Adv. Colloid Interface Sci.* **2017**, 247, 115–129.

(15) Raudino, A.; Raciti, D.; Corti, M. Anomalous behavior of ultra-low-amplitude capillary waves. A glimpse of the viscoelastic properties of Interfacial water? *Langmuir* **2017**, 33, 6439-6448.

(16) L. Cantu', A. Raudino, M. Corti An interferometric technique to study capillary waves. *Adv. Colloid Interface Sci.* **2017**, 247, 23-32.

(17) Corti, M.; Bonomo, M.; Raudino, A. New interferometric technique to evaluate the electric charges of gas bubbles in liquids. *Langmuir* **2012**, 28, 6060−6066.

(18) Corti, M.; Pannuzzo, M.; Raudino, A. Out of equilibrium divergence of dissipation in an oscillating bubble coated by surfactants. *Langmuir* **2014**, 30, 477−487.

(19) Corti, M.; Pannuzzo, M.; Raudino, A. Trapping of sodium dodecyl sulfate at the air-water Interface of oscillating bubbles. *Langmuir* **2015**, 31, 6277−6281.

(20) Brocca P.; Rondelli V.; Corti M.; Del Favero E.; Deleu M.; Cantu' L.. Interferometric investigation of the gas-phase monolayer of mono-rhamnolipid adsorbing at an oil/water interface. *J. Mol. Liquids* **2018,** 266, 687–691.

(21) Lamb, H. *Hydrodynamics*, 6th ed. Cambridge University Press: Cambridge, England, **1932**; reprinted by Dover: New York, **1993**.

(22) Bostwick, J. B.; Steen, P. H. Capillary oscillations of a constrained liquid drop. *Phys. Fluids* **2009**, 21, 032108

(23) Prosperetti, A. Linear oscillations of constrained drops, bubbles, and plane liquid surfaces. *Phys. Fluids* **2012**, 24, 032109.

(24) Maksimov, A.; Polovinka, Yu. A. Volume oscillations of a constrained bubble, Phys. Fluids **2013**, 25, 06210414.

(25) Rayleigh L. On the equilibrium of liquid conducting masses charged with electricity, *Phil. Mag.* **1882**, 14, 184-186.

Codice campo modificato

Codice campo modificato

Codice campo modificato

(26) Peters, T. Jr. Serum albumin. In *Advances in Protein Chemistry*, C. B. Anfinsen, J. T. Edsall, F. Richards, editors. Academic Press, New York **1985,** 161–245.

(27) Carter, C. D.; Ho, J. X. Structure of serum albumin. In Advances in Protein Chemistry. V. N. Schumaker, editor. Academic Press, New York. **1994**, 153–203.

(28) Osserman, E.; Canfield, R.; Beychak, S. Lysozyme, Academic Press, NY, **1974**

(29) Hanni-Ciunel, K.; Schelero, N.; von Klitzing, R. Negative charges at the air/water interface and their consequences for aqueous wetting films containing surfactants. *Faraday Discuss.* **2009**, 141, 41− 53.

(30) Salis, A.; Boström, M.; Medda, L.; Cugia, F.; Barse, B.; Parsons, D. F.; Ninham, B. W.; Monduzzi, M. Measurements and Theoretical Interpretation of Points of Zero Charge/Potential of BSA Protein. *Langmuir* **2011**, 27, 11597-11604.

(31) Salgin, S.; Salgın, U.; Bahadir, S. Zeta Potentials and Isoelectric Points of Biomolecules: The Effects of Ion Types and Ionic Strengths. *Int. J. Electrochem. Sci*. **2012,** 7, 12404-12414.

(32) Baler, K.; Martin, O. A.; Carignano, M. A.; Ameer, G. A.; Vila, J. A.; Szleifer, I. Electrostatic unfolding and interaction of Albumin driven by pH changes: a molecular dynamics study. *J. Phys. Chem. B* **2014**, 118, 921-930.

(33) Engelhardt, K.; Rumpel, A.; Walter, J.; Dombrowski, J.; Kulozik, U.; Braunschweig, B.; Peuke, W. Protein Adsorption at the Electrified Air−Water Interface: Implications on Foam Stability. *Langmuir* **2012**, 28, 7780−7787.

(34) Cho, G.; Narsimhan, E.; Franses, I. Adsorption Dynamics of Native and Pentylated Bovine Serum Albumin at Air–Water Interfaces: Surface Concentration/Surface Pressure Measurements. *J. Colloid Interface Sci*. **1997**, 191, 312–325.

(35) Miller, R.; Fainerman, V. B.; Wtistneck, R.; Krfigel, J. ; Trukhin, D. V. Characterisation of the initial period of protein adsorption by dynamic surface tension measurements using different drop techniques. *Colloids Surfaces A. Physicochem. Eng. Aspects* **1998,** 131, 225-230.

(36) Lu J. R.; Su T. J.; Thomas, R. K. Structural Conformation of Bovine Serum Albumin Layers at the Air–Water Interface Studied by Neutron Reflection. *J Colloid Interface* Sci **1999**, 213, 426 –437.

(37) Wang, J.; Buck, S. M.; Chen, Z. The effect of surface coverage on conformation changes of bovine serum albumin molecules at the air-solution interface detected by sum frequency generation vibrational spectroscopy. *Analyst* **2003**,128, 773−778.

(38) Lad, M.D.; Birembaut, F.; Matthew, J.M.; Frazier, R.A.; Green, R.J.; The adsorbed conformation of globular proteins at the air/water interface. *Phys Chem Chem Phys.* **2006**, 8, 2179-2186.

(39) Lakshmanana, M.; Dhathathreyana, A.; Miller, R. Synergy between Hofmeister effect and coupled water in proteins: Unusual dilational moduli of BSA at air/solution interface. *Colloids Surf A* **2008**, 324, 194–201.

(40) Wen X,; Franses E.I. Adsorption of bovine serum albumin at the air/water interface and its effect on the formation of DPPC surface film. *Colloids Surf A: Physicochem. Eng. Asp.* **2001,** 39190, 319–332.

(41) Wierenga P. A.; Meinders, M. B. J.; Egmond, M.R.; Voragen F.A.G.J.; de Jongh H. H. J. Protein Exposed Hydrophobicity Reduces the Kinetic Barrier for Adsorption of Ovalbumin to the Air−Water Interface. *Langmuir* **2003**, 19, 8964-8970.

(42) Holmes, A. M.; Holliday, S. G.; Clunie J. C.; Baird J. K. Electrophoretic mobility and zeta potential of lysozyme crystals. *Acta Cryst.* **1997**, D53, 456-457.

(43) Perriman, A. W.; White, J. W. Kinetics of adsorption of lysozyme at the air–water interface and the role of protein charge. *Physica B* **2006,** 385–386 716–718.

(44) Hunter, J. R.; Kilpatrick, P. K.; Carbonell, R. G. Lysozyme adsorption at the air/water interface. *J. Colloid Interface Sci.* **1990,** 137, 462-482.

(45) Alahverdjieva, V. S., Grigoriev, D. O.; Ferri, J. K.; Fainerman, V.B.; Aksenenko, E. V. ; Leser, M. E.; Michel, M.; Miller R. Adsorption behaviour of hen egg-white lysozyme at the air/water interface. *Colloids Surf A-Physicochem. Eng. Asp* **2008,** 323, 167–174.

(46) Graham, E. D.; Phillips, C. M. Proteins at liquid interfaces: I. Kinetics of adsorption and surface denaturation. *J. Colloid Interface Sci*. **1979,** 70, 403–413.

(47) Sundaram, S.; Ferri, J. K.; Vollhardt, D.; Stebe, K. J. Surface Phase Behavior and Surface Tension Evolution for Lysozyme Adsorption onto Clean Interfaces and into DPPC Monolayers: Theory and Experiment. *Langmuir* **1998**, 14, 1208-1218.

Codice campo modificato
Codice campo modificato
Codice campo modificato
Codice campo modificato
Codice campo modificato
Codice campo modificato
Codice campo modificato

(48) Krishnan, A.; Siedlecki, C. A.; Vogler, E. A. Traube-Rule Interpretation of Protein Adsorption at the Liquid−Vapor Interface. *Langmuir* **2003**, 19, 24, 10342-10352.

(49) Subramanyam, R.; Maldarelli, C. Fluorescence Evidence That a Phase Transition Causes the Induction Time in the Reduction in Dynamic Tension during Surfactant Adsorption to a Clean Air/Water Interface and a Kinetic–Diffusive Transport Model for the Phase-Induced Induction. *J. Colloid Interface Sci*. **2002**, 253, 377–392

(50) Miller, R.; Joos, P.; Fainerman, V. B. Dynamic surface and interfacial tensions of surfactant and polymer solutions. *Adv. Colloid Interface Sci.* **1994**, 49, 249-302.

(51) Prosser, A. J.; Franses, E. I. Adsorption and surface tension of ionic surfactants at the air–water interface: review and evaluation of equilibrium models. *Colloids Surf A: Physicochemical Eng. Asp.* **2001,** 178, 1–40.

(52) Miller, R.; Aksenenko, E. V.; Fainerman, V. B. Dynamic interfacial tension of surfactant solution. *Adv. Colloid Interface Sci.* **2017,** 247, 115–129

(53) Miller, R. Surface Tension Measurements with the Drop Profile Analysis Tensiometry—Consideration of the Surfactant Mass Balance in a Single Drop. *Colloids Interfaces* **2017**, 1, 1.

(54) Casandra A.; Chungb M-C., Noskovc B. A.; Shi-Yow Lin S-Y. Adsorption kinetics of sodium dodecyl sulfate on perturbed air-water interfaces. *Colloids Surf A: Physicochem. Eng. Asp.* **2017,** 518, 241–248.

(55) Kairaliyeva T.; Aksenenko E. V.; Mucic N.; Makievski A. V.; Fainerman V. B.; Miller R. Surface Tension and Adsorption Studies by Drop Profile Analysis Tensiometry. *J Surfact Deterg.* **2017,** 20, 1225–1241.

(56) Kinoshita, K.; Parra E.; Needham, D. Adsorption of ionic surfactants at microscopic air-water interfaces using the micropipette interfacial area-expansion method: Measurement of the diffusion coefficient and renormalization of the mean ionic activity for SDS. *J. Colloid Interface Sci*. **2017,** 504, 765–779.

(57) Leighton, T.G. The Acoustic Bubble, Academic Press, London, **1994**

(58) Saville, D. A. Electrohydrodynamic oscillation and stability of a charged drop. *Phys. Fluids* **1974,** 17, 54-60.

(59) Shaw, S. J.; Spelt, P. D. M.; Matar, O. K. Electrically induced bubble deformation, translation and collapse. *J. Eng. Math.* **2007**, 65, 291-310.

(60) Thaokar, R. M.; Deshmukh, S. D. Rayleigh instability of charged drops and vesicles in the presence of counterions. *Phys. Fluids* **2010,** 22, 034107.

(61) Padrino, J. C.; Funada T.; Joseph D. D. Purely irrotational theories for the viscous effects on the oscillations of drops and bubbles. *Int. J. Multiphase Flow*, **2008,** 34, 61-75.

(62) Diamant, H.; Andelman, D. Kinetics of surfactants adsorption at fluid-fluid interface. *J. Phys. Chem.* **1996,** 100, 13732-13742

(63) Adamson, A. W.; Gast, A. P. *Physical Chemistry of Surfaces*, John Wiley: New York, **1997**, Chapter 15.

(64) Ravera, F.; Loglio, G.; Kovalchuk, V.I. Interfacial dilational rheology by oscillating bubble/drop methods. *Curr. Opin. Colloid Interface Sci.* **2010**, 15, 217-228

(65) Bier, M.; de Graaf, J.; Zwanikken, J.; Van Roij, R. Curvature dependence of the electrolytic liquid-liquid interfacial tension. *J. Chem. Phys.* **2009**, 130, 024703-7.

(66) Bruhn, D. S.; Lomholt, M. A.; Khandelia, H. Quantifying the relationship between the curvature and electric potential in lipid bilayers. *J. Phys. Chem. B* **2016**, 120, 4812-4817.

(67) McAllister, I. W. Conductor curvature and surface charge density. *J. Phys. D* **1990**, 23, 359-362.

(68) Grebe, R.; Peterhansel, G.; Schmid-Shonbein, H**.** Change of local charge density by change of local mean curvature in biological bilayer membranes. *Mol. Cryst. Liq. Cryst.***1987***,* 152*,* 205-212.

(69) Pelekasis, N. A.; Tsamopoulos, J. A.; Manolis, G.D. Equilibrium shape and stability of charged and conducting drops. *Phys. Fluids* **1990**, 2, 1328-1340

(70) Deserno, M. Rayleigh instability of charged droplets in the presence of counterions**.** ***E****ur. Phys. J. E* **2001**, 6, 163-168.

(71) Tamashiro, M. N.; Schiessel, H. Rayleigh instability of charged aggregates: Role of the dimensionality, ionic strength and dielectric contrast. *Phys. Rev. E* **2006**, 74, 021412.

(72) Sammalkorpi, M.; Karttunen, N.; Haataja, M. Micelle fission through surface instability and formation of an interdigitated stalk. *J. Am. Chem. Soc.* **2008**, 130, 17977-17980.

(73) Bohr, N.; Wheeler, J. A. The mechanism of nuclear fission, *Phys. Rev.* **1939**, 56, 426-450.

(74) Ganan-Calvo A. M.; Montanero J. M. Revision of capillary cone-jet physics: Electrospray and flow focusing. *Phys. Rev. E*, **2009**, 79, 066305

(75) Kebarle, P. A brief overview of the present status of the mechanisms involved in electrospray mass spectrometry. *J. Mass Spectrom*. **2000**, 35, 804-817.

(76) Grimm, R.; Beauchamp, J. L. Dynamics of Field-Induced Droplet Ionization: Time-Resolved Studies of Distortion, Jetting, and Progeny Formation from Charged and Neutral Methanol Droplets Exposed to Strong Electric Fields. *J. Phys. Chem. B* **2005**, 109, 8244-8250.

(77) Jadhao, V.; Thomas, C. K.; Olvera de la Cruz, M. Electrostatics-driven shape transitions in soft shells. *Proc. Natl. Acad. Sci. USA* **2014**, 111, 12673-12678.

(78) Lin, S. Y.; McKeigue, K.; Maldarelli, C. Diffusion-controlled surfactant adsorption studied by pendant drop digitation. *AIChE J.* **1990**, 36, 1785-1795.

(79) Ward, A. F. H.; Tordai, L. Time dependence of boundary tension of solutions I. The role of diffusion in timr effectS. *J. Chem. Phys.* **1946**, 14, 453-461.

(80) Liggieri, L.; Ravera, F.; Passerone, A. A diffusion-based approach to mixed adsorption kinetics. *Colloids Surf A Physicochem Eng Asp*. **1996**, 114, 351-359.

(81) Abramowitz, M.; Stegun, I. A. *Handbook of Mathematical Functions*; Dover: NewYork, **1972**.

(82) Wertz, C. F.; Santore, M. M. Adsorption and reorientation of Lysozime on hydrophobic surfaces. *Langmuir* **2002**, *18*, 1190-1199.

(83) Daly, *S. M*.; Przybycien, T. M.; Tilton, R. D. Coverage dependent orientation of lysozyme adsorbed on silica. *Langmuir* **2003**, 19, 3848-3857**.**

(84) Rabe, M.; Verdes, D.; Seeger, S. Understanding protein adsorption phenomena at solid surfaces. *Adv. Colloid Interface Sci.* **2011**, 162, 87-106.

(85) Saykally, R. J. Two sides of the acid-base story. *Nature Chemistry* **2013**, 5, 82 EP

(86) Beattie, J. K.; Djerdjev, A. M.; Gray-Weale, A.; Kallay, N.; Lützenkirchen, J.; Preočanin, T.; Selmani, A. pH and the surface tension of water. J. *Colloid Int. Sci.* **2014**, 422, 54-57.

(87) Yan, X.; Delgado, M.; Aubry, J.; Gribelin, O.; Stocco, A.; Boisson-Da Cruz, F.;

Bernard, J.; Ganachaud, F. Central Role of Bicarbonate Anions in Charging Water/Hydrophobic Interfaces. *The Journal of Physical Chemistry Letters* **2018**, 9, 96-103

(88) Bohme, U.; Scheler, U. Effective charge of bovine serum albumin determined by electrophoresis NMR. *Chemical Physics Letters*, **2007,** 435, 342–345.

(89) Cho, D.; Narsimhan, G.; Franses, E.I. Adsorption Dynamics of Native and Alkylated Derivatives of Bovine Serum Albumin at Air–Water Interfaces. *J. Colloid Interface Sci.* **1996**, 178, 348-357.

(90) Najafi, A. S.; Drelich J.; Yeung, A.; Xu, Z.; Masliyah, J. A novel method of measuring electrophoretic mobility of gas bubbles. *Journal of Colloids Interface Science.* **2007,** 308, 344-350..

(91) Chen, X.; Yang, T.; Kataoka, S.; Cremer, P. S. Specific Ion Effects on Interfacial Water Structure near Macromolecules. *J. Am. Chem. Soc*. **2007**,129, 12272−12279.

(92) Smith, S. M. Strategies for the Purification of Membrane Proteins. *Methods Mol. Biol.* **2017**, 1485, 389-400.

(93) Du X.; Li Y.; Xia Y-L, Ai S-M.; Liang L.; Sang P.; Ji X-L.; Liu S-Q. Insights into Protein–Ligand Interactions: Mechanisms, Models, and Methods. *Int. J. Mol. Sci.* **2016,** 17, 144.

(94) Saponaro, A. (2018). Isothermal titration calorimetry: a biophysical method to characterize the interaction between label-free biomolecules in solution. Bio-protocol 8(15): e2957.

(95) Saponaro, A., Porro, A., Chaves-Sanjuan, A., Nardini, M., Rauh, O., Thiel, G. and Moroni, A. (2017). Fusicoccin activates KAT1 channels by stabilizing their interaction with 14-3-3 proteins. Plant Cell 29(10): 2570-2580.

(96) Saponaro, A., Cantini, F., Porro, A., Bucchi, A., DiFrancesco, D., Maione, V., Donadoni, C., Introini, B., Mesirca, P., Mangoni, M. E., Thiel, G., Banci, L., Santoro, B. and Moroni, A. (2018). A synthetic peptide that prevents cAMP regulation in mammalian hyperpolarization-activated cyclic nucleotide-gated (HCN) channels. Elife 7: 35753.

(97) Corti, M.; Raudino, A.; Cantu', L.; Theisen, J.; Pleines, M.; Zemb, T. Nanometric Surface Oscillation Spectroscopy of Water-Poor Microemulsion. *Langmuir.* **2018,** 34, 8154-8162.

Formattato: Inglese (Stati Uniti)

TOC

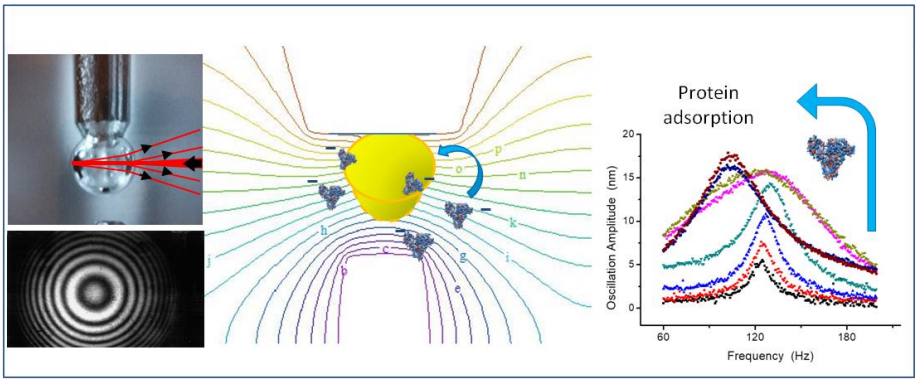
Protein
adsorption
Oscillation Amplitude (nm)
Frequency (Hz)
0
5
10
15
20
60
120
180